REVERSE TIME MIGRATION FOR VERTICAL TRANSVERSELY ISOTROPIC (VTI) MEDIA

D. H. HIEN[1], S. JANG[2], Y. KIM[2]
[1]University of Science and Technology
[2]Korea Institute of Geoscience and Mineral Resources

ABSTRACT: One of main assumption for solving wave equation either numerically or analytically is to compensate the anisotropic properties those are usually observed in the earth materials. Consequently, most conventional prestack depth migration techniques based on wave equation solution, are not sufficient for these anisotropic media. Asymptotic analysis of wave propagation in vertical transversely isotropic (VTI) media yields a dispersion relation of couple P- and SV wave modes that then can be converted to fourth order scalar partial difference (PDE) wave equation. By setting the shear velocity equal 0 and defining the auxilary function, the fourth order PDE acoustic wave equation for VTI media can be reduced to a system of coupled second order PDEs and then can be solved numerically by finite difference method (FDM). The result of this P wavefield simulation is kinematically similar to the one of elastic VTI wavefield simulation. Since the FDM approach can simulate the wavefield propagation in the VTI media, and reverse time migration (RTM) images the reflectors by using time extrapolation to synthesize source and receivers wavefield in the subsurface by FDM, the RTM technique is then promptly suggested to image the subsurface. The proposed algorithm has been shown the accuracy of subsurface imaging by VTI Marmousi synthetic example.

Keywords: Anisotropy, Vertically transverse isotropy, Finite difference method, Reverse time migratio.

INTRODUCTION

Seismic anisotropy occurs naturally in the earth materials due to i) Intrinsic anisotropy due to preferred orientation of anisotropic mineral grains or the shapes of isotropic minerals; ii) thin bedding of isotropic layers on a scale small compared to the wavelength (the layers may be horizontal or tilted) and iii) vertical or dipping fractures or micro-cracks. The certain anisotropy of a medium is produced by the combination of these factors (Thomsen, 1986). The transversely isotropic (TI) media is considered as the most common case to represent the shale formation that is composed of more than 75\% of the clastic fill of sediment basin in seismic exploration. Most shale formations are horizontally layered, yielding the a transversely isotropic medium with a vertical symmetric axis (VTI). Another common reason for TI symmetry is periodic thin layering on a small scale comparing to the predominant wavelength. The existence of anisotropy is hard to image the boundary below the TI layers and tends to shift the boundary up (Alkhalifah and Larner, 1994; Larner and Cohen, 1993; Vestrum et al., 1999; Isaac and Lawton, 1999), thus the consideration of anisotropy to the migration algorithm will overcome this limitation.

Prestack reverse time migration (RTM) requires zero lag cross correlation between the *back propagating wavefields* and *virtual sources* those are directly computed from finite difference method for solving wave equation (Chang and McMechan, 1986, Jang, 1996). By setting the shear velocity equal zero, Alkhalifah (2000) introduced an acoustic wave equation for VTI media from the dispersion relationship. Then, rotating the symmetric axis of VTI media to the angle of v yields the acoustic wave equation for the most general TI media (Fletcher et al., 2008). The wavefields resulted from finite difference solution of VTI acoustic wave equation show kinematically accurate to the one of real elastic wavefields. Consequently, the RTM for VTI media will be promptly suggested for overcoming the anisotropic effect to the isotropic RTM. The proposed algorithm will be verified by synthetic data.

ACOUSTIC VTI WAVE EQUATION

In the elastic anisotropic media, the wave equation (Aki and Rechards, 1980) is given as

$$\rho \frac{\partial^2 u_i}{\partial t^2} = f_i + c_{ijkl} \frac{\partial^2 u_k}{\partial x_l \partial x_j}, \quad (1)$$

where c_{ijkl} is stiffness tensor, f_i is external force, ρ is density and u_i is particles displacement vector.

To give an analytical description of plain waves in anisotropic media, the source term f_i is dropped down, thus the wave equation eq. (1) will be

$$\rho \frac{\partial^2 u_i}{\partial t^2} - c_{ijkl} \frac{\partial^2 u_k}{\partial x_l \partial x_j} = 0. \quad (2)$$

The trial solution of eq. (2) is

$$u_k = U_k e^{i\omega(n_j x_j - Vt)}, \quad (3)$$

where U_k are the components of the polarization vector U, ω is angular frequency, V is velocity that is usually called phase velocity, and n is unit vector orthogonal to plain wavefront (the wavefront satisfies $n_j x_j - Vt = const$).

Substitute plane wave in eq. (3) to plane wave equation eq. (2) leads to the equation called Christoffel equation for phase velocity V and polarization vector U

$$\begin{bmatrix} G_{11} - \rho V^2 & G_{12} & G_{13} \\ G_{21} & G_{22} - \rho V^2 & G_{23} \\ G_{31} & G_{32} & G_{33} - \rho V^2 \end{bmatrix} \begin{bmatrix} U_1 \\ U_2 \\ U_3 \end{bmatrix} = 0. \quad (4)$$

Here G_{ik} is the Christoffel matrix, which depends on the medium properties (stiffness tensor) and direction of wave propagation.

$$G_{ik} = c_{ijkl} n_j n_l \quad (5)$$

Using Kronecker 's symbolic δ_{ij} (δ_{ij}=1 if i=j, otherwise =0), the form of Christoffel equation eq. (4) can be rewritten as

$$[G_{ij} - \rho V^2 \delta_{ij}][U_i] = 0. \quad (6)$$

The Christoffel eq. (4) or (6) describes a standard 3×3 eigen value ρV^2 and eigen vector U problem for the symmetric matrix G. The eigen values are found from

$$det[G_{ij} - \rho V^2 \delta_{ij}] = 0, \quad (7)$$

which leads to the cubic equation for ρV^2.

For the case of VTI media, the Christoffel matrix elements will be

$G_{11}=c_{11}n_1^2+ c_{66}n_2^2+ c_{55}n_3^2$, (8)

$G_{11}=c_{66}n_1^2+ c_{11}n_2^2+ c_{55}n_3^2$, (9)

$G_{11}=c_{11}n_1^2+ c_{66}n_2^2+ c_{55}n_3^2$, (10)

$G_{11}=(c_{11}-c_{66})n_1n_2$, (11)

$G_{11}=(c_{13}+c_{55})n_1n_3$, (12)

$G_{11}=(c_{11}+c_{55})n_2n_3$. (13)

Since in the VTI media all planes containing the symmetry axis are equivalent, it is sufficient to study wave propagation in a single vertical plane. Choosing the $[x_1,x_3]$ plane and expressing unit vector **n** in terms of phase angle θ with the symmetry axis ($n_1=\sin\theta$, $n_2=0$, $n_3=\cos\theta$) and substituting equations from (8) to (13) into the Christoffel equation (6) yields the phase velocity of the transversely polarized mode $U_2 \neq 0$, $U_1=U_3=0$

$$V_{SH}(\theta) = \sqrt{\frac{c_{66}\sin^2\theta + c_{55}\cos^2\theta}{\rho}}, \quad (14)$$

and in-plane polarized modes (P-SV) are described by the first and third equation of eq. (6)

$$\begin{bmatrix} c_{11}n_1^2 + c_{55}n_3^2 - \rho V^2 & (c_{13} + c_{55})n_1 n_3 \\ (c_{13} + c_{55})n_1 n_3 & c_{55}n_1^2 + c_{33}n_3^2 - \rho V^2 \end{bmatrix} \begin{bmatrix} U_1 \\ U_3 \end{bmatrix} = 0. \quad (15)$$

Using the Fourier domain representation of the wavefront normal vector $n_1=Vk_x/\omega$ and $n_3=Vk_z/\omega$, where k_x, k_z and ω is wave number along x, z axises and angular frequency, respectively, and defining the normalized the stiffness $a_{ij}=c_{ij}/\rho$, the coupled P-SV wave system from eq. (15) becomes

$$\begin{bmatrix} a_{11}k_x^2 + a_{55}k_z^2 - \omega^2 & (a_{13} + a_{55})k_x k_z \\ (a_{13} + a_{55})k_x k_z & a_{55}k_x^2 + a_{33}k_z^2 - \omega^2 \end{bmatrix} \begin{bmatrix} U_1 \\ U_3 \end{bmatrix} = 0. \quad (16)$$

Setting the determinant of eq. (16) to zero yields

$$0 = \omega^4 - [(a_{11} + a_{55})k_x^2 + (a_{33} + a_{55})k_z^2]\omega^2 + a_{11}a_{55}k_x^4 + a_{13}a_{55}k_z^4 + [a_{11}a_{33} + a_{55}^2 - (a_{13} + a_{55})^2]k_x^2 k_z^2. \quad (17)$$

Because the rotational symmetry of VTI media is around the vertical axis, eq. (17) can be rotated into any other vertical plane by just replacing k_x^2 by $k_x^2+k_y^2$, the dispersion relation will be the velocities can be substituted for stiffness using the following relationship

$$0 = \omega^4 - [(a_{11} + a_{55})(k_x^2 + k_y^2) + (a_{33} + a_{55})k_z^2]\omega^2 + a_{11}a_{55}(k_x^2 + k_y^2)^2 + a_{13}a_{55}k_z^4 + [a_{11}a_{33} + a_{55}^2 - (a_{13} + a_{55})^2](k_x^2 + k_y^2)k_z^2 \quad (18)$$

$$a_{11} = V_{px}^2, \tag{19}$$

$$a_{33} = V_{p0}^2, \tag{20}$$

$$a_{55} = V_{s0}^2, \tag{21}$$

$$a_{55} + \frac{(a_{11}+a_{55})^2}{a_{33}-a_{55}} = V_{nmo}^2. \tag{22}$$

where V_{p0} is vertical P-wave velocity; $V_{px} = V_{p0}\sqrt{1+2\varepsilon}$ is horizontal P-wave velocity; $V_{nmo} = V_{p0}\sqrt{1+2\delta}$ is the P-wave normal move out velocity; V_{s0} is vertical SV wave velocity; ε and δ is dimensionless Thomsen's parameters.

With these substitution and multiplying both two sides with wavefield $\mathbb{U}$ in frequency wave number domain, eq. (18) becomes

$$0 = \omega^4\mathbb{U} - \left[\left(V_{px}^2 + V_{s0}^2\right)\left(k_x^2 + k_y^2\right) + \left(V_{p0}^2 + V_{s0}^2\right)k_z^2\right]\omega^2\mathbb{U} + \left\{V_{px}^2V_{s0}^2\left(k_x^2 + k_y^2\right)^2 + V_{p0}^2V_{s0}^2k_z^4 + \left[V_{p0}^2\left(V_{px}^2 - V_{nmo}^2\right) + V_{s0}^2\left(V_{p0}^2 + V_{nmo}^2\right)\right]\left(k_x^2 + k_y^2\right)k_z^2\right\}\mathbb{U}. \tag{23}$$

Taking the inverse Fourier transform of eq. (23) by using the relations $i\omega \leftrightarrow \frac{\partial}{\partial t}$; $ik_x \leftrightarrow \frac{\partial}{\partial x}$ and $ik_z \leftrightarrow \frac{\partial}{\partial z}$ yields the 4th order partial derivative equation (PDE)

$$0 = \frac{\partial^4 U}{\partial t^4} - \left(V_{px}^2 + V_{s0}^2\right)\left(\frac{\partial^4 U}{\partial x^2\partial t^2} + \frac{\partial^4 U}{\partial y^2\partial t^2}\right) - \left(V_{p0}^2 + V_{s0}^2\right)\frac{\partial^4 U}{\partial z^2\partial t^2} + V_{px}^2V_{s0}^2\left(\frac{\partial^4 U}{\partial x^4} + 2\frac{\partial^4 U}{\partial x^2\partial y^2} + \frac{\partial^4 U}{\partial y^4}\right) + V_{p0}^2V_{s0}^2\frac{\partial^4 U}{\partial z^4} + \left[V_{p0}^2\left(V_{px}^2 - V_{nmo}^2\right) + V_{s0}^2\left(V_{p0}^2 + V_{nmo}^2\right)\right]\left(\frac{\partial^4 U}{\partial x^2\partial z^2} + \frac{\partial^4 U}{\partial y^2\partial z^2}\right). \tag{24}$$

By setting the shear velocity equal to zero and adding the source function f, the wave equation eq. (24) becomes

$$f = \frac{\partial^4 U}{\partial t^4} - V_{px}^2\left(\frac{\partial^4 U}{\partial x^2\partial t^2} + \frac{\partial^4 U}{\partial y^2\partial t^2}\right) - V_{p0}^2\frac{\partial^4 U}{\partial z^2\partial t^2} + V_{p0}^2\left(V_{px}^2 - V_{nmo}^2\right)\left(\frac{\partial^4 U}{\partial x^2\partial z^2} + \frac{\partial^4 U}{\partial y^2\partial z^2}\right), \tag{25}$$

that is called *acoustic wave equation for VTI media*. Eq. (25) will be the scalar acoustic equation for istropic media if the ε and δ equals to 0.

Introducing the auxiliary function $W = \frac{\partial^2 U}{\partial t^2}$, eq. (25) in two dimentions becomes a coupled equations

$$W = \frac{\partial^2 U}{\partial t^2}$$

$$\frac{\partial^2 W}{\partial t^2} = V_{px}^2\frac{\partial^2 W}{\partial x^2} - V_{p0}^2\frac{\partial^2 W}{\partial z^2} + V_{p0}^2\left(V_{px}^2 - V_{nmo}^2\right)\frac{\partial^4 U}{\partial x^2\partial z^2} + f \tag{26}$$

.

Using the second-order finite difference approach, the partial derivative wavefield can be approximated, therefore the wavefield can be estimated.

Figure 1 shows the wavefield at 0.25 time step generated from acoustic wave equation eq. (25), while figure 2 shows the wavefield at 0.25 time step of vertical component of wavefield generated directly by numerical solution of elastic anisotropic wave equation eq. (1) for VTI media. The VTI media has the P wave velocity of 3000m/sec, epsilon of 0.2 and delta of 0.1 and the Ricker wavelet with 20Hz peak frequency is used as source fuction and located at the center of the model. Comparatively, the P waves generated from acoustic and elastic wave equation are kinematically similar. Dynamically, they differ considerably. Both elastic and acoustic wavefields have secondary arrival. The elastic wavefield secondary arrival is S wave wavefront while the diamond shaped acoustic one is a quasi S wave wavefront (Grechka et al., 2004).

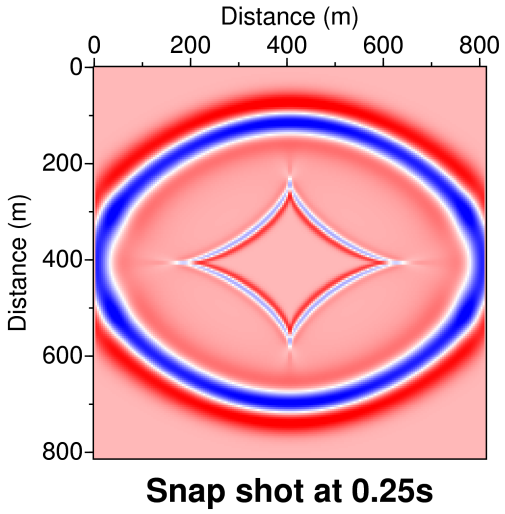

Figure 1 Wavefield generated from VTI acoustic wave equation at the 0.25 second

REVERSE TIME MIGRATION FOR VTI MEDIA

The principle of RTM is zero lag cross correlation between the virtual source and back propagating wavefields those are directly calculated from FDM for acoustic wave equation (Jang, 1996; Shin et al., 2001). Since the FDM can be applied to simulate the acoustic wave equation for VTI media and following the same approach of RTM for acoustic media, the RTM can be further developed for the VTI media as derived in the follows.

The general assembled system of finite element or finite difference equations can be written as (Marfurt, 1984)

$$M\ddot{U}(t) + CU(t) = F, \tag{27}$$

where M, C and F is the global mass matrix, global stiff matrix and load vector. The subsurface image created by zero lag crosscorrelation between the partial derivative wavefield and shot gathers leads to the mathematical derivation of isotropic RTM (Shin and Chung, 1999; Shin et al., 2001; Tarantola, 1984; Pratt, 1994). The same approach can be used for the VTI media and generalized to the other kinds of anisotropic media.
In the frequency domain, the discretized wave equation eq. (27) is written as

$$K(p)\mathbb{U}(\omega,p) - \omega^2\mathbb{U}(\omega,p) = \mathbb{F}(\omega), \tag{28}$$

where ω is angular frequency; $\mathbb{U},\mathbb{F}$, is Fourier transform of U and f, respectively. Eq. (28) suggests to recover the

wavefield

$$\mathbb{U}(\omega,p) = S(p)^{-1}\mathbb{F}(\omega), \tag{29}$$

where

$S(p)=K(p)-\omega^2M(p)$

Taking the partial derivative both side of eq. 28 respect to single physical parameter, say p_1, yields

$$K(p)\frac{\partial U(p)}{\partial p_1} - \omega^2 M(p)\frac{\partial U(p)}{\partial p_1} = -\left(\frac{\partial K(p)}{\partial p_1} - \omega^2\frac{\partial M(p)}{\partial p_1}\right)\mathbb{U}(p) \tag{30}$$

Taking a look on eq. (30) and comparing to the wave eq. (29), we may see that these two equations have the same form of the Laplacian operator, the difference is the source function. The source function of eq. (29) is normally given or assumes to be known, on the other the hand, the expression $\left(\frac{\partial K(p)}{\partial p_1} - \omega^2\frac{\partial M(p)}{\partial p_1}\right)\mathbb{U}(p)$, calculated by wavefield and physical parameters, is called virtual source term. Consequently, partial derivative wave field can be calculated by FDM and virtual source that is calculated by wavefields and physical parameters.

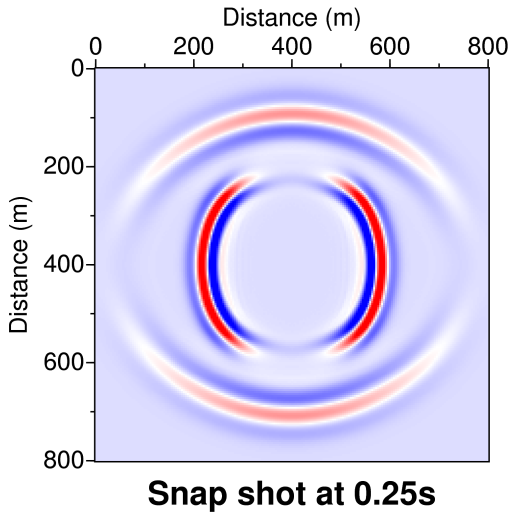

Figure 2 Wavefield generated from VTI elastic wave equation at the 0.25 second

Multiplying eq. (30) by the inverse of $K(p)-\omega^2M(p)$ gives

$$\frac{\partial U(p)}{\partial p_1} = -S(p)^{-1}\left(\frac{\partial K(p)}{\partial p_1} - \omega^2\frac{\partial M(p)}{\partial p_1}\right)\mathbb{U}(p), \tag{31}$$

The subsurface are normally divided into grid size with NN nodals as shown in figure 3, and the partial derivative of wavefield respect to physical parameters has to be calculated at each grid points, thus the matrix notation of eq. (31) is given by

$$\begin{bmatrix} \frac{\partial U_1}{\partial p_1} \\ \vdots \\ \frac{\partial U_{NN}}{\partial p_1} \end{bmatrix} = S(p)^{-1}\begin{bmatrix} f_1^1 \\ \vdots \\ f_1^{NN} \end{bmatrix}, \tag{32}$$

where the virtual sources distribution f_1 is given by

$$\begin{bmatrix} f_1^1 \\ \vdots \\ f_1^{NN} \end{bmatrix} = \left(\frac{\partial K(p)}{\partial p_1} - \omega^2\frac{\partial M(p)}{\partial p_1}\right)\begin{bmatrix} \mathbb{U}_1 \\ \vdots \\ \mathbb{U}_{NN} \end{bmatrix}.$$

Taking the transpose of eq. (32) results in:

$$\begin{bmatrix} \frac{\partial U_1}{\partial p_1} & \cdots & \frac{\partial U_{NN}}{\partial p_1} \end{bmatrix} = \begin{bmatrix} f_1^1 & \cdots & f_1^{NN} \end{bmatrix} S(p)^{-1^T}. \quad (33)$$

Similarly, the partial derivative of wavefield respect to the other physical parameters p_2, p_3,…,p_m are given as

$$\begin{bmatrix} \frac{\partial U_1}{\partial p_2} & \cdots & \frac{\partial U_{NN}}{\partial p_2} \end{bmatrix} = \begin{bmatrix} f_2^1 & \cdots & f_2^{NN} \end{bmatrix} S(p)^{-1^T}. \quad (34)$$

$$\begin{bmatrix} \frac{\partial U_1}{\partial p_m} & \cdots & \frac{\partial U_{NN}}{\partial p_m} \end{bmatrix} = \begin{bmatrix} f_m^1 & \cdots & f_m^{NN} \end{bmatrix} S(p)^{-1^T}. \quad (35)$$

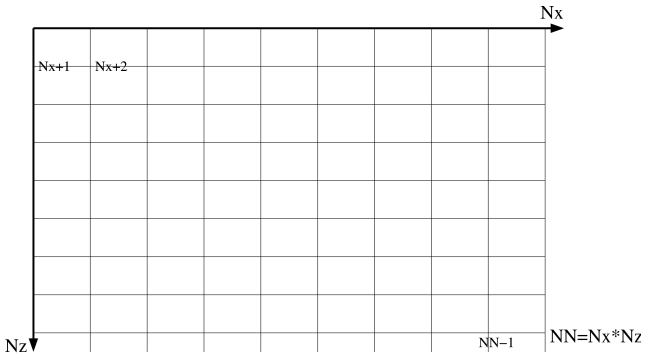

Figure 3. Conversation of nodal connection, Nx, Nz indicate for the number grids in x and z direction, NN indicates for total number of grids (after Shin (1988))

In summary, the partial derivative matrix will be

$$\begin{bmatrix} \frac{\partial U_1}{\partial p_1} & \cdots & \frac{\partial U_{NN}}{\partial p_1} \\ \vdots & \cdots & \vdots \\ \frac{\partial U_1}{\partial p_m} & \cdots & \frac{\partial U_{NN}}{\partial p_m} \end{bmatrix} = \begin{bmatrix} f_1^1 & \cdots & f_1^{NN} \\ \vdots & \cdots & \vdots \\ f_m^1 & \cdots & f_m^{NN} \end{bmatrix} S(p)^{-1^T}. \quad (36)$$

The number of observation data are much smaller than the number of grids, thus the null values should be added to observation data vector to handle zero lag crosscorrelation of partial derivative wavefield and observation data that is given as the follows

$$\begin{bmatrix} \frac{\partial U_1}{\partial p_1} & \cdots & \frac{\partial U_{NN}}{\partial p_1} \\ \vdots & \cdots & \vdots \\ \frac{\partial U_1}{\partial p_m} & \cdots & \frac{\partial U_{NN}}{\partial p_m} \end{bmatrix} \begin{bmatrix} D_1 \\ \vdots \\ D_N \\ 0 \\ \vdots \\ 0 \end{bmatrix}$$

$$= \begin{bmatrix} f_1^1 & \cdots & f_1^{NN} \\ \vdots & \cdots & \vdots \\ f_m^1 & \cdots & f_m^{NN} \end{bmatrix} S(p)^{-1^T} \begin{bmatrix} D_1 \\ \vdots \\ D_N \\ 0 \\ \vdots \\ 0 \end{bmatrix} \quad (37)$$

To demonstrate the accuracy of imaging condition for VTI media by zero lag crosscorrelation of partial derivative wavefield and observation data, the simple VTI media (figure 4) is used. The fist layer with the P wave velocity of 1500 m/s is isotropic, while the second layer is VTI with the P wave velocity of 2500 m/s, epsilon of 0.25 and delta of 0.1. Figure 5 shows the shot gather that is achieved from the numerical solution of eq. \ref{vti-acwe}. For imaging of this shot gather, the partial derivative of wavefields respect to P wave velocity at every grid points have to be calculated. Figure 7 shows some examples of the partial derivative calculation at six dot points given in figure 4. Before that the virtual sources calculation results are shown in figure 6. The zero lag crosscorrelation of partial derivative of wavefield respect to P wave velocity and shot gathers at the grid points along the center lines of the model is shown in figure 8a, while figure 8b show the remaining part of image profile after cutting all the value shallower than 100m. The figure 8b shows very clearly that at the boundary of two layer where the velocity changes, the value of zero lag crosscorrelation changes significantly or it creates the high amplitude in the profile comparatively to the surrounding points. Gathering these zero lag crosscorrelation results at all grid points of the velocity model enables to image the subsurface as seen in figure 9. The image shows very clearly the velocity boundary.

The zero lag crosscorrelation of partial derivative wavefield and observation data method enables to image clearly the subsurface for not only the acoustic isotropic media but also for the VTI media, however it requires extremely high computing cost. Thus, it is not sufficient for the real data set which the velocity models consist of much larger number of grids than the example one.

Because the $S(p)^{-1^T}$ is symmetric, thus the zero lag

crosscorrelation of partial derivative wavefields and shot gathers can be rewritten as

$$\begin{bmatrix} \frac{\partial U_1}{\partial p_1} & \cdots & \frac{\partial U_{NN}}{\partial p_1} \\ \vdots & \cdots & \vdots \\ \frac{\partial U_1}{\partial p_m} & \cdots & \frac{\partial U_{NN}}{\partial p_m} \end{bmatrix} \begin{bmatrix} D_1 \\ \vdots \\ D_N \\ 0 \\ \vdots \\ 0 \end{bmatrix} = \begin{bmatrix} f_1^1 & \cdots & f_1^{NN} \\ \vdots & \cdots & \vdots \\ f_m^1 & \cdots & f_m^{NN} \end{bmatrix} \begin{bmatrix} b_1 \\ \vdots \\ b_N \\ 0 \\ \vdots \\ 0 \end{bmatrix}, \quad (38)$$

where

$$\begin{bmatrix} b_1 \\ \vdots \\ b_N \\ 0 \\ \vdots \\ 0 \end{bmatrix} = S(p)^{-1^T} \begin{bmatrix} D_1 \\ \vdots \\ D_N \\ 0 \\ \vdots \\ 0 \end{bmatrix}$$

is called back propagating wavefield. Thus, the zero lag cross correlation of virtual source and back propagation, that is principle of reverse time migration for VTI media, is able to image the subsurface. Figure 10 shows the result of this imaging method for the physical parameters and shot gather given in figure 4 and figure 5, respectively. As seen in figure 10, the boundary is very clear to allocate and the image looks similar to the one in figure 9 and accurately matches to the physical parameters model (figure 4).

REVERSE TIME MIGRATION FOR VTI MARMOUSI MODEL

Marmousi model is wel-known with the phase of comp*lex geological structure*. The huge amount of folding and faulting induced in this model have created a rather interesting distribution of velocity anomalies and discontinuities. Thus, the Marmousi model served as a calibration tool (Audebert et al., 1994; Versteeg and Lailly, 1991; Rekdal and Biondi, 1994; Shin and Min, 1996) used to verify the various migration and inversion algorithms through the years. The Marmousi data set was generated at the Institute Francais du Petrole (IFP), and used for the workshop on practical aspects of seismic data inversion at the 1990 EAEG meeting in Copenhagen, where different groups (contractors, universities, and oil companies) applied their proffered imaging tools on this data set. Detailed accounting of what transpired at the workshop is given by (Versteeg and Grau, 1990) and (Versteeg and Lailly, 1991). The original Marmousi data set was generated using a 2-D acoustic finite-difference modeling program. The Marmousi model is, however, based on the simplistic assumption that the Earth subsurface is isotropic, despite the many arguments (Banik, 1984; Harris et al., 1994; Alkhalifah, 1997) that suggest otherwise.

The existence of such an acoustic wave equation (eq. (25)) for VTI media allows us to generate realistic synthetic data in the VTI complex models. An example of the ever popular VTI Marmousi model (Alkhalifah, 1997) was created by introducing new two dimensionless Thomsen's parameters and shear wave velocity model as shown in figure 11. Here we can see, the deepest part of Marmousi model, below the discontinuities where the anticline trap consists of low velocity zone representing for hydrocarbon is kept as isotropic layer. The hydrocarbon accumulation anticline trap is target of most of migration algorithms. Consequently, to apply the proposed algorithms to migrate the VTI Marmousi model data set is very significant to verify the accuracy of proposed algorithm.

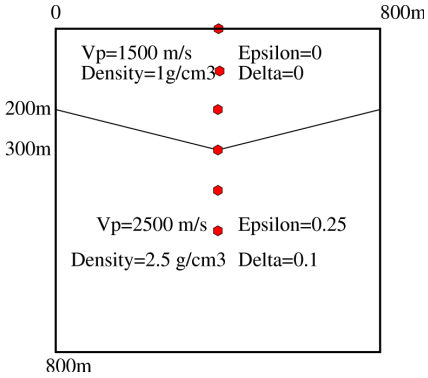

Figure 4 Input velocity and Thomsen's parameters. The dots indicate for example of positions to calculate the virtual source and partial derivative wavefields

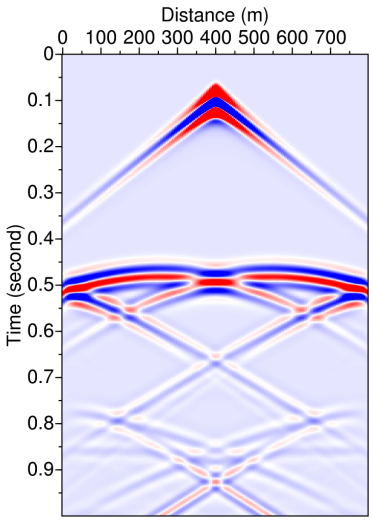

Figure 5 Shot gather generated by FDM for VTI media given in figure 4

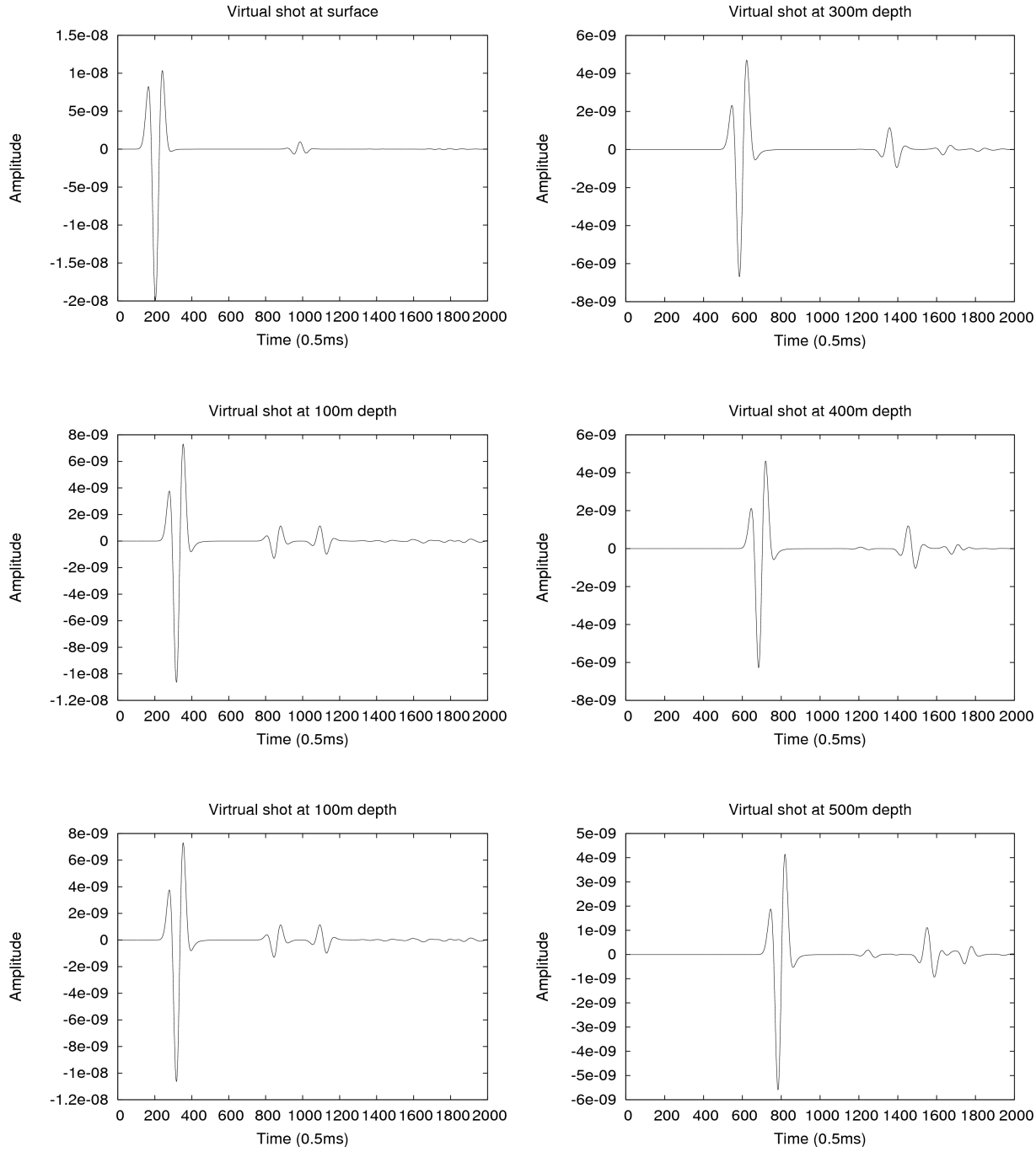

Figure 6 Virtual shot calculation at different positions showing in figure 4

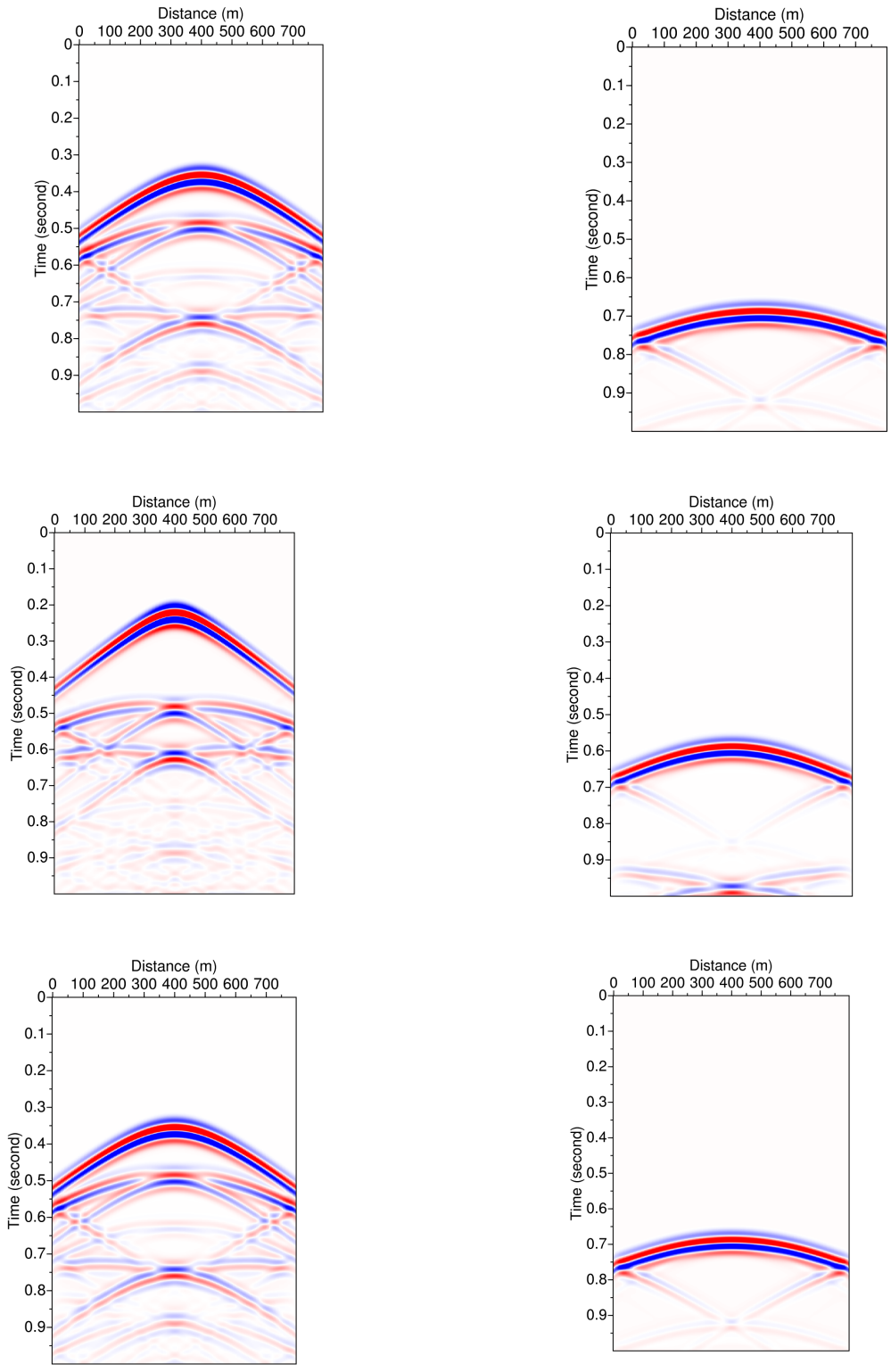

Figure 7 Partial derivative wavefield calculation at different locations showing in figure 4

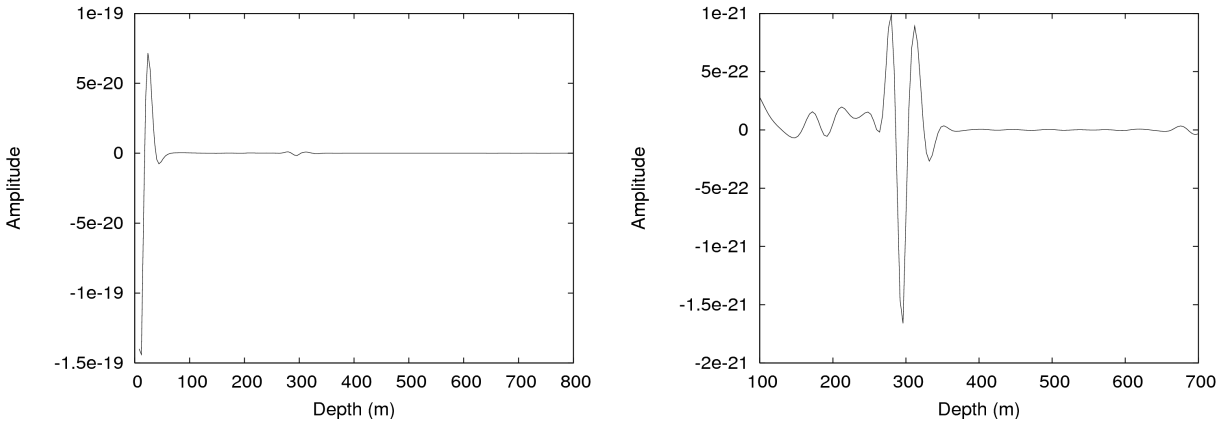

Figure 8 Result of zero lag crosscorrelation between partial derivative wavefields respect to P wave velocity showing examples in figure 6 and shot gather data showing in figure 5

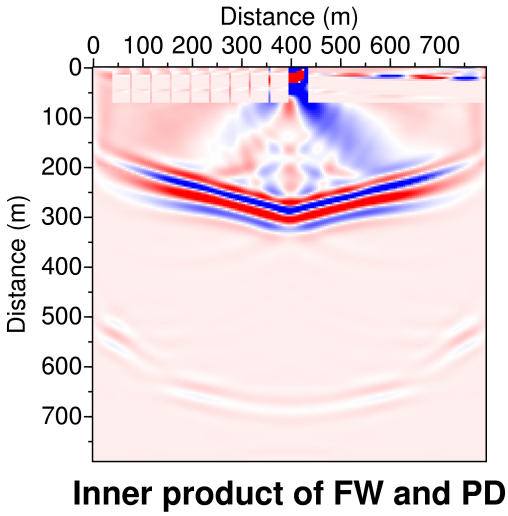

Figure 9 Result of zero lag crosscorrelation of partial derivative wavefields and shot gathers data

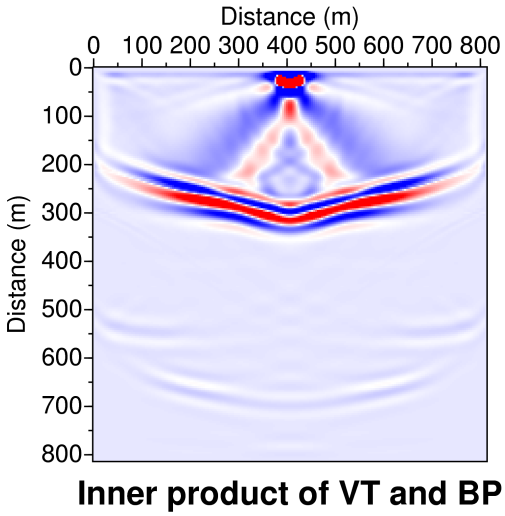

Figure 10 Result of zero lag crosscorrelation of virtual source and back propagating wavefields

Since the Thomsen's parameters are given, the horizontal P wave and NMO P wave velocity are simply calculated. Then, the FDM method can be adopted to the given VTI Marmousi model. The model is divided into 240×737 grids; both horizontal and vertical grid size is 12.5 m for forward modeling. The VTI Marmousi dataset consists of 240 shots with 135 traces per shot. The near offset is 200 m; both receiver and shot interval is 25 m. The first shot location is at the position of 3000 m. Figure 12 shows common shot gathers #50, 100, 150 and 200 corresponding to shot locations of 3750, 4500, 5250 and 6000 m, respectively. In the shot gathers data, the moveout no longer appears hyperbolic, which directly reflects the complexity of the model. Alkhalifah, 1997 use Kirchhoff prestack depth migration for isotropically migrating the VTI Marmousi data set. The migrated section showed the reservoir location slightly shifted and many shallow faults were improperly imaged as a result of ignoring anisotropy. Here, applying the VTI RTM for the VTI Marmousi data set shot by shot then summing up all 240 single imaging gather of 240 shot create full migrated section of VTI Marmousi data as displayed in figure 13. The reservoir and other geological structures including main faulting and folding systems are very clearly imaged. However, the sediment layers of the shallow part is rather poorly imaged. This limitation can be ignored if the preprocessing steps such as filtering and deconvolution before and after migration are applied.

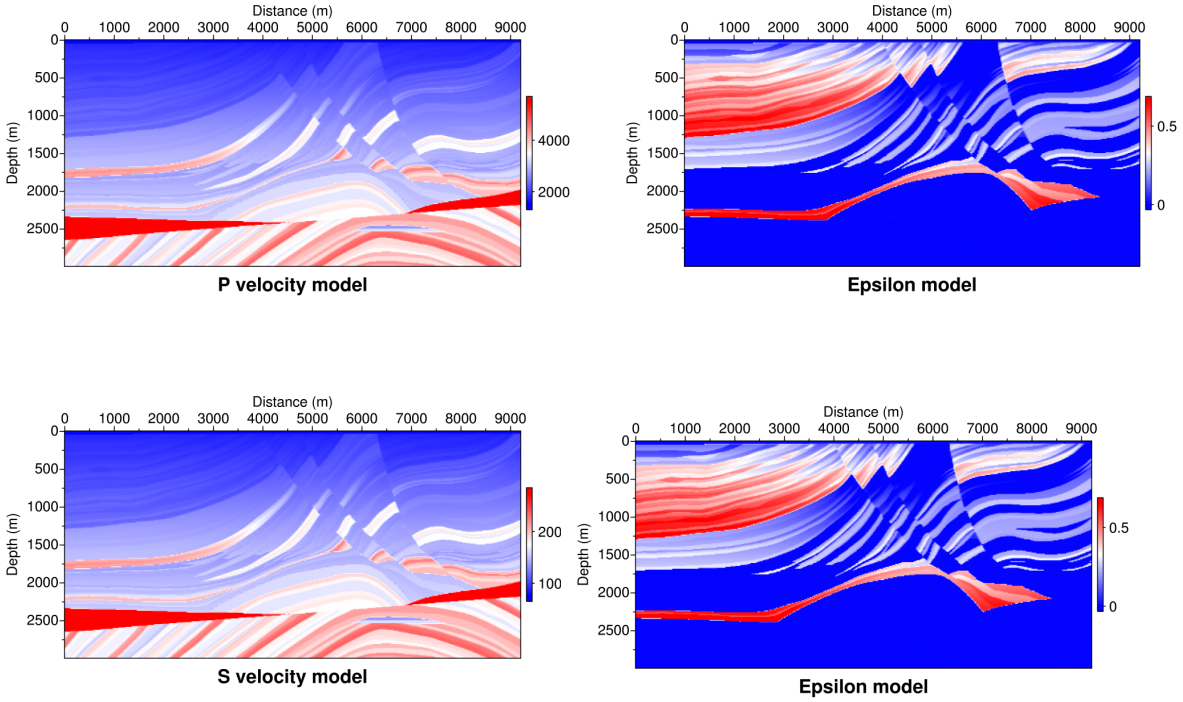

Figure 11. Input velocities and Thomsen's parameter of VTI Marmousi model

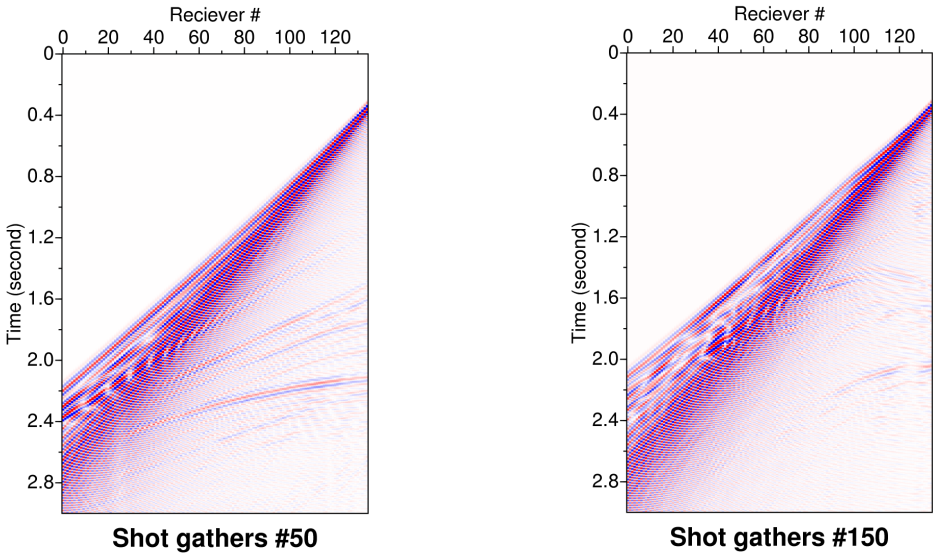

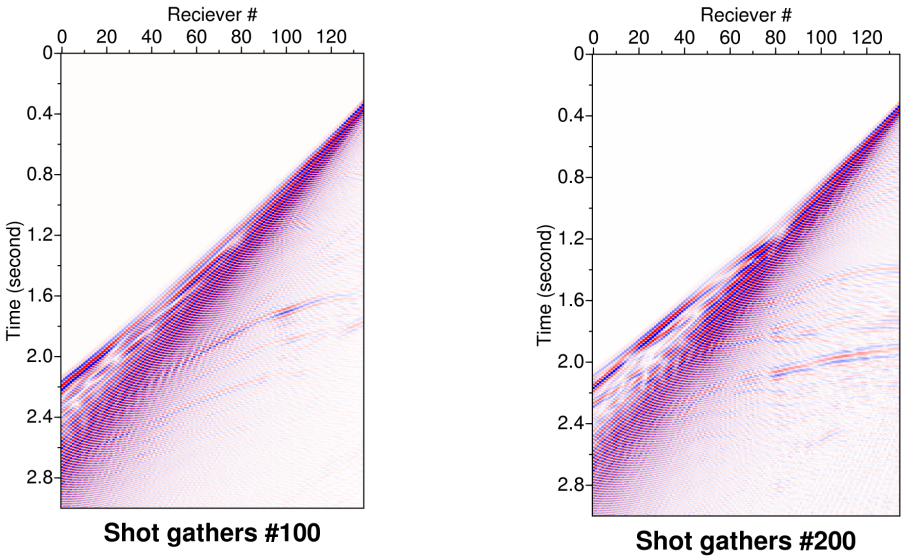

Figure 12 Examples of shot gathers from forward modeling as input for back propagating wavefield

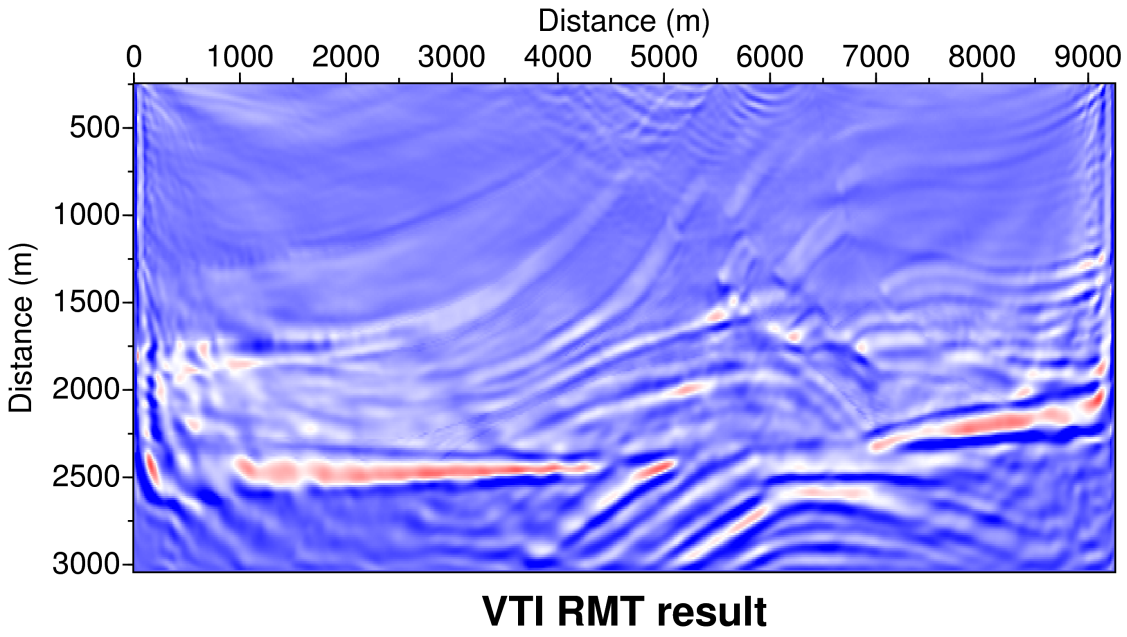

Figure 13 Result of VTI RTM as after summation of 240 single image gathers

CONCLUSION

Setting shear velocities equal 0 of the dispersion relationship yields the acoustic anisotropic wave equation for VTI media that can be solved numerically faster than elastic anisotropic wave equation. The result of numerical simulation of acoustic anisotropic wave equation shows kinematically reasonable to the elastic anisotropic one. Thus, it can be used for migration purpose since the primary events in the recorded shot gathers are almost recognized the P waves.

Both zero lag crosscorrelation methods enable to image the subsurface not only for acoustic isotropic media but also for VTI media. The computing time of RTM is much less than the zero lag crosscorrelation of partial derivative and observation data, so it can handle bigger size of velocity model of the real seismic data set.

The principle of reverse time migration by zero lag crosscorrelation of virtual shot and back propagating wavefields for VTI media has been proven comprehensively and verified by VTI Marmousi model.

Thus, this imaging method can be further developed for the other complicated anisotropic media and it should be recommended for further study.

ACKNOWLEDGMENTS

This research was supported by the Basic Research Project of the Korea Institute of Geoscience and Mineral Resources (KIGAM) funded by the Ministry of Knowledge and Economy.

REFERENCES

Aki, K., and P. G. Rechards, (1980), Quantitative seismology: theory and methods: W. H. Freeman and Co.

Alkhalifah, T., (1997), An anisotropic marmousi model: SEP report, 265–283.

———, (2000), An acoustic wave equation for anisotropic media: Geophysics, 65, 1239–1250.

Alkhalifah, T., and K. Larner, (1994), Migration error in transversely isotropic media: Geophysics, 59, 1405–1418.

Audebert, F., B. Biondi, D. Lumley, T. Rekdal, and H. Urdaneta, (1994), Marmousi traveltime computation and imaging comparisions: SEP, 80, 47–66.

Banik, N. C., (1984), Velocity anisotropy of shales and depth estimation of the north sea basin: Geophysics, 49, 1411–1419.

Chang, W. F., and G. A. M. Mechan, (1986), Reverse time migration in of offset vertical seismic data profiling data using the excitation time imaging condition: Geophysics, 51, 1514–1524.

Fletcher, R., X. Du, and P. J. Fowler, (2008), A new pseudo acoustic wave equation for tti media: 78th *Annual International Meeting*, SEG, Expanded abstract, 2082–2086.

Grechka, V., L. Zhang, and J.W. Rector, (2004), Shear waves in acoustic anisotropic media: Geophysics, 69, 1045–1055.

Harris, J. M., L. Dahlhous, and R. Mechelena, (1994), P wave anisotropy in shales from crosswell data: 64th *Annual International Meeting,* SEG, Expanded abstract, 1125–1128.

Isaac, J. H., and D. C. Lawton, (1999), Imaging mispositioning due to dipping ti media: A physical seismic modeling study: Geophysics, 64, 1230–1238.

Jang, S., (1996), Imaging of the earth interior using cross correlation: *PhD thesis*, Hanyang University.

Larner, K., and J. K. Cohen, (1993), Migration error in transversely isotropic media with linear velocity variation in depth: Geophysics, 58, 1454–1467.

Marfurt, K. J., (1984), Accuracy of finte difference and finite element modeling of scalar and elastic wave equation: Geophysics, 49, 533–549.

Pratt, R. G., (1999), Seismic waveform inversion in the frequency domain, part 1: Theory verification in a physical scale model: Geophysics, 64, 888–901.

Rekdal, T., and B. Biondi, (1994), Paraxial ray tracing in the Marmousi model: 64th *Annual International Meeting,* SEG, Expanded abstract.

Shin, C., S. Jang, and D. Min, (2001), Improved amplitude preservation for prestack depth migration by inverse scattering theory: *Geophysical Prospecting*, 49, 592–606.

Shin, C. S., 1988, Nonlinear elastic wave inversion by blocky parameterization: *PhD thesis*, University of Tulsa.

Shin, C. S., and S. Chung, (1999), Understanding cmp stacking hyperpola in terms of partial derivative wavefield: Geophysics, 64, 1774–1782.

Shin, C. S., and D. J. Min, (2006), Waveform inversion using a logarithmic wavefield: Geophysics, 71, R31–R42.

Tarantola, A., (1984), Inversion of seismic reflection data in the acoustic approximation: Geophysics, 49, 1259–1266.

Thomsen, L., (1986), Weak elastic anisotropy: Geophysics, 51,1954–1966.

Versteeg, R., and G. Grau, (1990), Practical aspects of seismic data inversion, the marmousi experiences: *52nd Annual Meeting*, EAEG, Procceding.

Versteeg, R., and P. Lailly, (1991), Eaeg workshop report: Practical aspects of seismic data inversion: First Break, 9.

Vestrum, R. W., D. C. Lawton, and R. Schmid, (1999), Imaging structure below dipping ti media: Geophysics, 64, 1239–1246.